ORIGINAL ARTICLE

JBMR®

Modifications to Nano- and Microstructural Quality and the Effects on Mechanical Integrity in Paget's Disease of Bone

Elizabeth A Zimmermann,[1,2] Till Köhne,[1] Hrishikesh A Bale,[3] Brian Panganiban,[3] Bernd Gludovatz,[2] Joszef Zustin,[4] Michael Hahn,[1] Michael Amling,[1] Robert O Ritchie,[2,3] and Björn Busse[1,2]

[1]Department of Osteology and Biomechanics, University Medical Center Hamburg-Eppendorf, Hamburg, Germany
[2]Materials Sciences Division, Lawrence Berkeley National Laboratory, Berkeley, CA, USA
[3]Department of Materials Science and Engineering, University of California, Berkeley, CA, USA
[4]Institute of Pathology, University Medical Center Hamburg-Eppendorf, Hamburg, Germany

ABSTRACT

Paget's disease of bone (PDB) is the second most common bone disease mostly developing after 50 years of age at one or more localized skeletal sites; it is associated with severely high bone turnover, bone enlargement, bowing/deformity, cracking, and pain. Here, to specifically address the origins of the deteriorated mechanical integrity, we use a cohort of control and PDB human biopsies to investigate multiscale architectural and compositional modifications to the bone structure (ie, bone quality) and relate these changes to mechanical property measurements to provide further insight into the clinical manifestations (ie, deformities and bowing) and fracture risk caused by PDB. Here, at the level of the collagen and mineral (ie, nanometer-length scale), we find a 19% lower mineral content and lower carbonate-to-phosphate ratio in PDB, which accounts for the 14% lower stiffness and 19% lower hardness promoting plastic deformation in pathological bone. At the microstructural scale, trabecular regions are known to become densified, whereas cortical bone loses its characteristic parallel-aligned osteonal pattern, which is replaced with a mosaic of lamellar and woven bone. Although we find this loss of anisotropic alignment produces a straighter crack path in mechanically-loaded PDB cases, cortical fracture toughness appears to be maintained due to increased plastic deformation. Clearly, the altered quality of the bone structure in PDB affects the mechanical integrity leading to complications such as bowing, deformities, and stable cracks called fissure fractures associated with this disease. Although the lower mineralization and loss of aligned Haversian structures do produce a lower modulus tissue, which is susceptible to deformities, our results indicate that the higher levels of plasticity may compensate for the lost microstructural features and maintain the resistance to crack growth. © 2014 American Society for Bone and Mineral Research.

KEY WORDS: PAGET'S DISEASE OF BONE; PATHOMECHANISM; FRACTURE RISK; BONE QUALITY; MECHANICAL PROPERTIES; COLLAGEN CHARACTERISTICS

Introduction

Paget's disease of bone (PDB) was first described by Sir James Paget in 1876 after observing distinct proportion changes and deformities in patients' bones.[1] Today, PDB is the second most common bone disease behind osteoporosis. The disease is usually triggered after the age of 50 years possibly by genetic and/or environmental factors.[2,3] PDB has a high prevalence in western European countries as well as regions around the world formerly colonized by people from western European descent.[4,5]

PDB localizes at one or more skeletal sites, most commonly the pelvis, spine, femur, and tibia,[2,3,5–7] leading to outwardly observable abnormalities in the bone's size and shape. Although approximately 90% of patients do not have any symptoms, 10% of patients with PDB suffer from pain in bones, joints, and muscles; headaches; hearing loss; gait disturbances; compression of nerves; local temperature increases; and secondary osteoarthritis.[5,8–10] However, the hallmark diagnostic feature of PDB under X-ray examination is the reorganization of the bone emphasized through a combination of osteolytic, sclerotic, and deformed bone regions indicating hypervascularity, trabecular densification, and cortical thickening (Fig. 1*A*).[8,11,12] This pronounced disease pattern is accompanied by blood serum markers of bone remodeling showing abnormally high alkaline phosphatase activity and bone-specific alkaline phosphatase activity,[10,13] which are indicators of excessive bone remodeling.

At the bone cellular level, where previously a delicate balance of bone resorption by osteoclast cells and bone deposition by osteoblast cells produced healthy bone, changes in the osseous cell activity after the onset of PDB reflect a defective bone remodeling pattern. The appearance of abnormally shaped osteoclasts, so called "giant osteoclasts" characteristic of PDB, are

Received in original form June 11, 2014; revised form August 4, 2014; accepted August 7, 2014. Accepted manuscript online August 12, 2014.
Address correspondence to: Björn Busse, PhD, Department of Osteology and Biomechanics, University Medical Center, Lottestrasse 59, 22529 Hamburg, Germany. E-mail address: b.busse@uke.uni-hamburg.de

Journal of Bone and Mineral Research, Vol. 30, No. 2, February 2015, pp 264–273
DOI: 10.1002/jbmr.2340

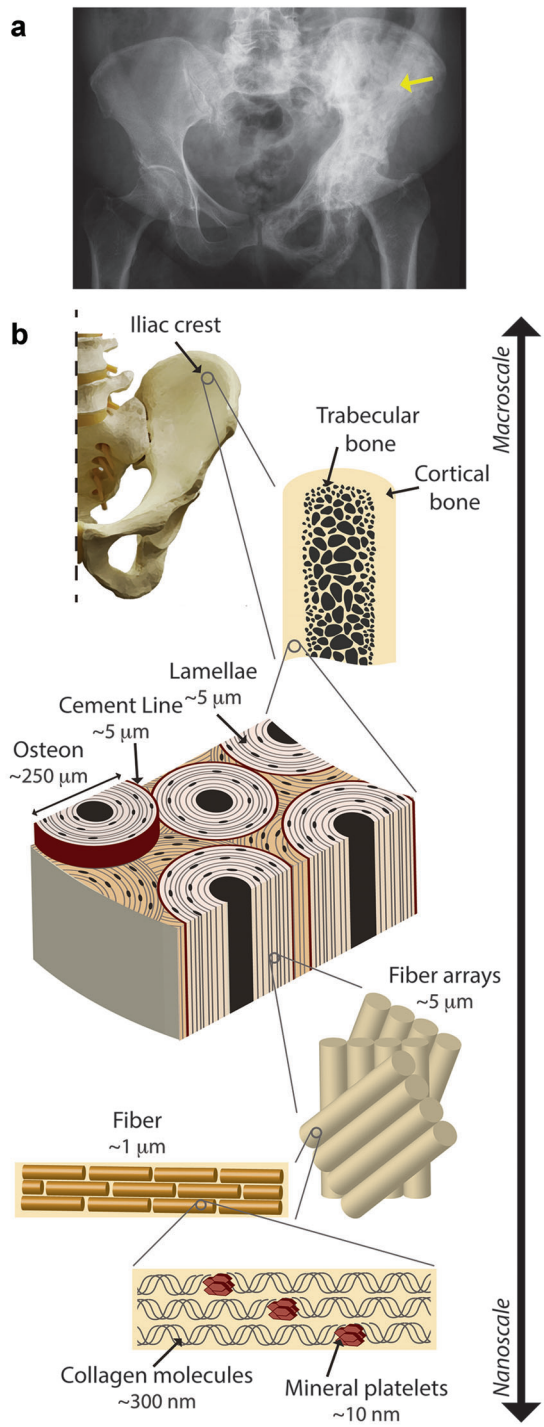

Fig. 1. Hierarchical structure of bone. (*A*) Radiologic signs of PDB in the area marked by the yellow arrow, where the bone has a larger density and size. (*B*) In this study, biopsies from the iliac crest were used to analyze the structural and mechanical properties in control and PDB cases. At this skeletal site, the bone architecture consists of a dense cortical shell surrounding a porous trabecular core. At the microstructural length-scale, the cortical bone consists of osteons, which have a hypermineralized cement line delineating their outer boundary and lamellae concentrically surrounding a central vascular cavity termed the Haversian canal. The lamellae are composed of arrays of fibers, which are composed of fibril arrays. The fibril is a composite of collagen molecules and mineral platelets. PDB = Paget's disease of bone.

related to enhanced bone resorption followed by osteoblastic overstimulation causing increased bone volume,[3,14] which contributes to the typical enlargement of the affected bones. Essentially, both increased osteoclast and osteoblast activity cause the striking high bone turnover in PDB.[3,15] As a result, increased proportions of rapidly synthesized and non-organized collagen matrix are deposited followed by a brief mineralization period,[15] producing a bone matrix with a structure resembling a mosaic of woven bone.[15–17]

The changes in bone remodeling as well as the resulting outwardly observable changes in whole-bone geometry at diseased skeletal sites indicate a shift in bone quality. Bone quality describes the integrity of bone's hierarchical structural features (Fig. 1*B*), which span collagen molecules (~300 nm) and mineral nanoparticles (~10 nm) at small-length scales to cylindrical features called osteons at the size-scale of 100s of microns in cortical bone to the interconnecting architecture in trabecular bone. Bone's mechanical integrity arises from the quality of the bone structure and how it resists deformation and fracture.[18–21] The hierarchical structure contributes to the mechanical integrity in terms of *intrinsic* and *extrinsic* mechanisms that resist deformation and fracture. Specifically, the *intrinsic* material resistance results in bone's inherent stiffness, strength, and resistance to crack initiation. The intrinsic resistance originates from the composition and assembly of bone's constituents at small-length scales and how these features promote or restrict plasticity (whereas elastic deformation refers to the stretching of bonds, plastic or inelastic deformation implies permanent, irreversible deformation). In bone, the primary intrinsic mechanisms are thought to be fibrillar sliding and sacrificial bonding, and modifications, eg, in the cross-linking or mineralization profiles, are thought to impact the generation of plasticity at this length-scale.[22] In contrast, the *extrinsic* material resistance results in bone's resistance to the growth of a crack. The extrinsic resistance originates from larger-length scales on the microstructural scale that are large enough to stop/interfere with crack growth. In effect, extrinsic mechanisms shield the growth of cracks through crack deflection or bridging mechanisms.[22]

Epidemiological studies have quantified fracture risk in cohorts of patients with PDB.[10,23–26] Various studies have found a slight to no increase in overall fracture risk (because PDB localizes at one or more skeletal sites, it is important to differentiate between fracture risk at pathological bone sites and overall fracture risk) in patients with PDB.[23,24] However, higher rates of fracture have been reported through pathological bone, even after bisphosphonate treatment.[23,26] Even though fracture events at pathological skeletal sites are uncommon (occurring in ~2% of patients), fracture does represent a concern in patients with PDB and may be accompanied by further fracture-related complications, such as subsequent fracture, nonunion of fractured site, and pseudofracture or fissure fractures.[23,24,26–28] Fractures at pathological skeletal sites are commonly transverse (ie, "chalk-stick" fractures) and preceded by the presence of incomplete fractures, termed pseudofractures or fissure fractures.[12,29] Regions with severe bowing and deformity commonly contain the fissure fractures, which occur on the convex side of the bone under tensile stress and contribute to the sensation of bone pain.[28,30,31]

Because PDB clearly disrupts the mechanical integrity of bone tissue, leading to bowing, deformity, and fissure fractures in clinical cases, our aim here was to use a cohort of human iliac crest bone biopsies from control and PDB cases to experimentally characterize the structure, composition, and mechanical properties. Thus, modifications to the multiscale bone structure in PDB

were related to the mechanical properties to investigate the fracture risk and the origins of reduced mechanical integrity (ie, bowing, deformities, cracking) commonly found in clinical cases.

Materials and Methods

Study design

The objective of this study was to characterize the alterations to the structure and composition as well as the mechanical properties of bone from healthy patients and those with PDB. Here, 49 control and 49 PDB methylmethacrylate (MMA)-embedded iliac crest biopsies were obtained from the Hamburg Bone Registry at the University Medical Center, Hamburg-Eppendorf, Germany. The control samples stem from a previous bone histomorphometry study and did not show any sign of mineralization defects or pathologic tissue.[32,33] All individuals suffering from cancer, renal diseases, primary hyperparathyroidism, and/or showing any other circumstances, such as immobilization or hospitalization, potentially leading to secondary bone diseases, were excluded from the study. The PDB biopsies were taken to diagnose the source of abnormal X-rays and/or scintigraphy in patients with bone pain and/or suspicion of breast and prostate cancer. Therefore, the PDB cases exhibited pathological tissue at this skeletal region and had previously not been treated for PDB. The study was approved by the Lawrence Berkeley National Laboratory (BUA-120). The PDB cohort consisted of 19 females and 30 males with an average age of 72.2 ± 7.3 years. The control cohort consisted of 16 females and 33 males with an average age of 59.3 ± 7.3 years.

Histomorphometry

Prior to embedding, the samples were first fixed in 4% phosphate-buffered formaldehyde and then dehydrated in an ascending ethanol series (80%, 90%, 94%, 96%, 100% ethanol). Undecalcified specimens were infiltrated in two steps with MMA solutions (Merck, Darmstadt, Germany). Afterward, the polymerization of destabilized MMA augmented with N,N dimethyl-p-toluidine (DMPT) as an initiator/catalyst took place under a N_2 saturated atmosphere. The polymerization of resin in all of the samples' voids took place at a temperature of 4 °C. Static histomorphometry was performed on toluidine blue or Giemsa-stained undecalcified sections. The following parameters were measured according to ASBMR standards[34] with an Osteo-Measure histomorphometry system (Osteometrics, Atlanta, GA, USA) and a Zeiss microscope (Carl Zeiss, Jena, Germany): bone volume (BV/TV), trabecular thickness (Tb.Th), trabecular number (Tb.N), trabecular separation (Tb.Sp), osteoid volume (OV/BV), osteoid surface (OS/BS), osteoclast number (N.Oc/B.Pm), osteoclast surface (Oc.S/BS), osteoblast number (N.Ob/B.Pm), and osteoblast surface (Ob.S/BS).

Quantitative backscattered electron imaging

Although undecalcified histology is able to capture soft tissue and bone cells, backscattered electron imaging has the capability to focus on the different degrees of mineralization within the bone tissue.[35–38] Here, the bone mineral density distribution (BMDD) was measured via quantitative backscattered electron imaging (qBEI) on 46 controls and 49 PDB cases. The measurements were performed at 20 kV and 580 pA (LEO 435 VP; Leo Electron Microscopy Ltd., Cambridge, UK) with a constant working distance of 20 mm using a solid state backscattered electron detector (BSE Detector, Type 202; K.E. Developments Ltd., UK). The electron beam was kept constant at 580 pA using a Faraday cup (MAC Consultants Ltd., UK). The signal amplification (brightness and contrast) was calibrated during the entire procedure by keeping measurements of carbon and aluminum standards (MAC Consultants Ltd., UK).[39] The gray-level histograms of bone were standardized using a threshold routine (Image J 1.42; National Institutes of Health, Bethesda, MD, USA). The obtained gray values were transformed into calcium weight percentages as described.[33,39] We evaluated the value (Ca mean), standard deviation (SD) (Ca width), and peak (Ca peak) of the calcium distribution, which refer to the mean calcium content, the heterogeneity of the calcium content, and the most frequent calcium content, respectively.[38,40] Additionally, we calculated the mean value of the distributions' 5th and 95th percentiles, which were 16.54 and 27.15 wt % Ca, respectively. For every distribution curve, we also evaluated the portion left of the mean 5th percentile (Ca low) and right of the mean 95th percentile (Ca high). These BMDD parameters represent the area of low and highly mineralized bone, respectively.

Fourier transform infrared spectroscopy

To assess the quality of the bone matrix, Fourier transform infrared (FTIR) spectroscopy was performed on 5 control and 5 PDB cases. From the embedded bone sections, 5-μm-thick sections were cut with a microtome to acquire FTIR spectra in transmission with a FTIR imaging system (Spotlight 400; Perkin Elmer, Waltham, MA, USA). Over a specified bone area, spectra were acquired at 6.25-μm intervals over the spectral range of 570 to 4000 cm^{-1} at a spectral resolution of 4 cm^{-1} and 128 scans. In total, at least 8000 pixels of bone (roughly $560 \times 560\ \mu m^2$) were analyzed per sample in both the trabecular and cortical compartments. Spectra were analyzed using a custom program in Matlab (MathWorks, Natick, MA, USA). Each spectrum was baseline corrected and the contribution from the embedding material was subtracted from the measured spectrum.

At each pixel, area ratios were calculated from the spectra to quantify the mineral-to-matrix ratio, carbonate-to-phosphate ratio, and 1660/1690 cm^{-1} collagen crosslink ratio.[41–43] The mineral-to-matrix ratio was measured as the area ratio of the phosphate υ_1 (915 to 1180 cm^{-1}) to amide I peaks (1590 to 1725 cm^{-1}). The carbonate-to-phosphate ratio was measured as the area ratio of the carbonate (850 to 900 cm^{-1}) to phosphate υ_1 peaks (915 to 1180 cm^{-1}). The collagen crosslink ratio was determined by peak-fitting the amide I and II bands between 1490 and 1725 cm^{-1}. Specifically, the amide I and II bands were smoothed with a Savitzky-Golay filter using 21 points and a 2nd degree polynomial. For the 1660/1690 cm^{-1} collagen crosslink ratio, the second derivative of the bands was used to determine the locations of nine subbands and the collagen crosslink ratio was then correlated to the area ratio of the 1660 cm^{-1} to 1690 cm^{-1} subbands.[42]

The average mineral-to-matrix, carbonate-to-phosphate, and collagen crosslink ratios were obtained for each case by calculating the average and SD of the parameters from each pixel over the area of interest.

Polarized light microscopy

Histological sections were toluidine blue–stained and observed under linearly polarized light. Collagen fibrils or bundles of fibrils, which are cut longitudinally and run parallel to the polarizer or analyzer plane, appear bright on the dark background, whereas cross-sectioned fibrils or fibers appear dark. The application of

linearly polarized light on histological sections qualitatively distinguished between woven and lamellar bone within the specimen taken from control and PDB cases.[44]

Nanoindentation

The mechanical properties of 14 control and 14 PDB cases were assessed via nanoindentation measurements. The embedded and polished biopsy specimens were indented with a Berkovich tip in a Triboindenter (Hysitron, Minneapolis, MN, USA) perpendicular to the cross-section. The indent was loaded at a rate of 100 μN/s. When a peak load of 600 μN was reached, the load was held for 10 s and then the sample was unloaded at the same rate. Three sets of 10 indent points were performed in a field with at least a 5-μm separation. The Young's modulus and the hardness of the bone samples were acquired from the nanoindentation measurements.

Reference point indentation

The mechanical properties of 10 controls and 10 PDB cases were analyzed with reference point indentation (RPI) measurements. Microindentations perpendicular to the cross-section were made on polished embedded bone biopsies with a Biodent Reference Point Indenter (ActiveLife Tech, Inc., Santa Barbara, CA, USA). A BP2 probe was used to apply an indentation force of 6 N at an indentation rate of 2 Hz with 10 indentations per measurement cycle. Three indents were made in the cortical compartment of each iliac crest biopsy, and the first-cycle indentation distance, indentation distance increase, first-cycle creep indentation distance, and average energy dissipated were reported.

In situ fracture toughness tests

Four control and 3 PDB cases fulfilled the criteria for a valid fracture mechanics experiment according to ASTM standard 1820 with an external cortex of roughly 12 mm in length and 1.4 mm in width.[45] The samples were polished into beams, notched with a water-irrigated low-speed saw, and then the saw-cut notch was sharpened to a crack tip radius of roughly 10 μm by polishing the root of the notch with a razor blade irrigated with 0.5 μm diamond solution. The features of the bone structure (ie, osteons, cement lines, mineralized collagen fibrils, etc.) are predominantly aligned in a certain orientation. Because of this anisotropy, bone fracture toughness can be measured either parallel (ie, longitudinal orientation) or perpendicular (ie, transverse orientation) to the structure's orientation; here, the bone fracture toughness was measured in the transverse orientation. The surface of the sample was polished to a 0.5-μm finish and the samples were hydrated in Hanks' Balanced Salt Solution (HBSS) for at least 12 hours prior to testing. The toughness of the notched samples was tested with a Gatan Microtest 2kN bending stage (Gatan, Abington, UK) in a S-4300SE/N variable pressure scanning electron microscope (Hitachi America, Pleasanton, CA, USA), allowing continuous observation of the crack length on the sample's surface throughout mechanical testing.

The linear elastic stress-intensity factor was measured as a function of crack growth following standard ASTM 1820.[45] Corrections were made to the load to account for the porosity in the control and pagetic samples. A change in porosity will reduce the load bearing area and increase the load in the material as follows: $P_{corr} = P/(1-p)$, where P is the experimentally measured load, P_{corr} is the porosity-corrected load, and p is the porosity, which was measured on the bulk sample via synchrotron micro–computed tomography (μCT).

Corrections were also made to the stress intensity to account for crack deflection. The average deflection angle, θ, was measured through the thickness of each sample via X-ray μCT. The globally applied mode-I stress intensity, K_I, was converted to the local mode I, k_1, and mode II, k_2, stress intensities at the crack tip by the following relationship for in-plane tilted cracks: $k_1 = a_{11}(\theta)K_I + a_{12}(\theta)K_{II}$ and $k_2 = a_{21}(\theta)K_I + a_{22}(\theta)K_{II}$, where $a_{ij}(\theta)$ are mathematical functions dependent on the angle of crack deflection, θ.[46] The local stress intensities can then be converted to an effective stress intensity using the following relationship based on the strain energy release rate: $K_{eff} = ({k_1}^2 + {k_2}^2)^{1/2}$. Assuming a yield strength of 100 MPa and the initiation toughness of $K = 1.15$ MPa $m^{1/2}$, the minimum sample thickness for plane-strain conditions of 0.33 mm and minimum in-plane dimensions of 0.007 mm to satisfy the criterion for small-scale yielding were both met to ensure validity of the test.

3D synchrotron μCT

The crack paths from the fracture tests were assessed in the cortical regions of control and PDB samples by microtomography. The microtomography was performed after mechanical testing to avoid changes in mechanical properties associated with high doses of irradiation.[20] Briefly, at beamline 8.3.2 at the Advanced Light Source (Lawrence Berkeley National Laboratory, Berkeley, CA, USA), scans were conducted at 17 keV with monochromatic X-rays at a minimum sample-to-detector distance of 50 mm and a 600-ms exposure at a 1.8-μm/pixel spatial resolution around the crack path. Tomography slices were reconstructed with Octopus (Octopus v8, IIC UGent) from 1440 exposures acquired over 180-degree sample rotation in 0.125-degree angular increments and visualized in Avizo 6.1 (Visualization Sciences Group, Inc.).

Statistics

Results are presented as means ± SD. Statistical analysis was performed with OriginPro 8 (OriginLab Inc.). To test for differences between the study groups, we used the unpaired two-sided t test on normally distributed data. The normal distribution of the data was tested using the Kolmogorov-Smirnov test. Values of $p \leq 0.05$ were considered statistically significant. For data that was not normally distributed, a nonparametric two-sided Mann-Whitney test was used.

Results

Characterization of mineral and collagen quality

Here, we find significant changes in the composition and quality of the Paget's bone structure at small-length scales. qBEI of the BMDD indicates a distinctly lower mineral content in PDB cases (Fig. 2*A*–*C*). From the distribution of the mineral content, the histogram showing the frequency of each mineral density can be used to quantify the Ca mean, Ca peak, Ca low, Ca high, and Ca width (heterogeneity). Here, in the PDB cases, the Ca mean and Ca peak values are both ~19% lower (Fig. 2*A*–*C*, Table 1) and contained six times more bone with a low mineral density distribution as well as 86% less bone with a high BMDD (Fig. 2*A*–*C*, Table 1). The PDB cases also had a 17% greater degree of heterogeneity in bone mineralization, as measured through the width of the histograms (Fig. 2*A*–*C*, Table 1). All of these BMDD parameters indicate a prominent lower degree of mineralization in the PDB cases.

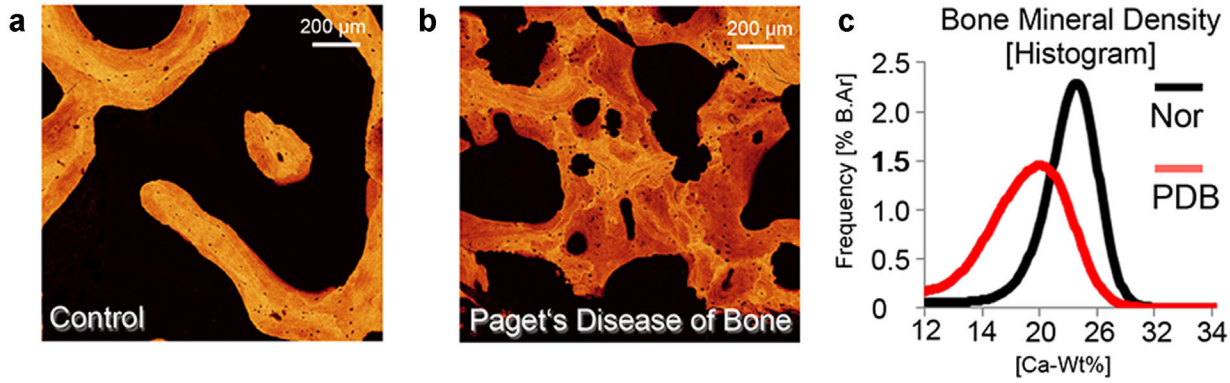

Fig. 2. Small length-scales: Quantitative backscattered electron imaging. The BMDD was assessed in the control and PDB cases with qBEI, where the gray values reflect the calcium content. The stark differences in the BMDD are clearly visible in the pseudo-colored backscattered electron images of (*A*) control and (*B*) PDB samples, as well as the (*C*) histogram of the density distribution. BMDD = bone mineral density distribution; PDB = Paget's disease of bone; qBEI = quantitative backscattered electron imaging; B.Ar = bone area.

FTIR was also used to characterize the collagen and mineral quality (Fig. 3*A*–*D*), where the peak area ratios correlate to specific bone quality parameters: mineral-to-matrix ratio (MMR), carbonate-to-phosphate ratio (CPR), and 1660/1690 cm^{-1} collagen crosslink ratio. FTIR measurements confirm a 12% lower MMR in PDB (control 2.96 ± 0.20, PDB 2.59 ± 0.13, $p = 0.009$) (Fig. 3*B*) and also indicate a 15% lower CPR (control 0.0104 ± 0.0006, PDB 0.0088 ± 0.0005, $p = 0.003$) (Fig. 3*C*). The CPR corresponds to carbonate substitution for phosphate in the mineral lattice and generally increases with tissue age (ie, the relative age of the osteons). For the organic component, FTIR showed a significantly higher collagen crosslink ratio in PDB (control 3.40 ± 0.41, PDB 3.94 ± 0.18, $p = 0.040$) (Fig. 3*D*), which corresponds to changes in the collagen's secondary structure and/or an increased presence of noncollagenous proteins (eg, osteonectin, osteocalcin, and osteopontin) in PDB.[47,48] Thus, the qBEI and FTIR results indicate changes to the composition and quality of the bone tissue in PDB resulting in a lower, heterogeneous bone mineralization and a younger tissue age.

Characterization of trabecular and cortical morphology

In the trabecular region of the iliac crest, static histomorphometry reveals elevated bone turnover and a denser bone volume in the PDB cases (Table 2). Indeed, the PDB cases have a significant increase in bone volume (Table 2) measured through a 2.5-fold increase in trabecular bone volume (BV/TV), threefold increase in trabecular number (Tb.N), and nearly 4.5-fold decrease in trabecular spacing (Tb.Sp). However, the trabecular thickness did not significantly change. Thus, the bone volume increases through the creation of new trabeculae and not through apposition or growth of preexisting trabeculae.[3] Additionally, the PDB cases had a significant increase in bone formation measured through increases in osteoid as well as osteoclast and osteoblast numbers (Table 2).

Table 1. BMD Distribution Indices

BMD distribution indices	Control	PDB	*p*
Ca mean [wt %]	22.8 ± 0.8	18.4 ± 1.6	<0.001
Ca peak [wt %]	23.9 ± 0.7	19.4 ± 2.2	<0.001
Ca low [% B.Ar]	5.16 ± 2.16	32.31 ± 14.55	<0.001
Ca high [% B.Ar]	5.09 ± 2.75	0.72 ± 1.06	<0.001
Ca width [Δwt %]	3.44 ± 0.22	4.03 ± 0.24	<0.001

The values are reported as mean ± SD.

In the cortical structure, synchrotron X-ray CT images reveal that the parallel Haversian canals characteristic of healthy human bone are replaced by disorganized clusters of porosity (ie, regions of hypervascularity) without a certain directional pattern (Fig. 4*A*, *B*). Polarized light microscopy (Fig. 4*C*, *D*) shows that these clusters are a patchwork of lamellar and woven bone, which is characteristic of PDB,[15–17] whereas the control cases have a normal lamellar structure.[49,50] Thus, on the microstructural level, the sandwich structure of the iliac crest, consisting of a trabecular core surrounded by a cortical frame in control cases, is replaced by a dense clumsy bone structure that lacks a well-defined directional orientation of collagen fibers and osteons.

Mechanical properties

Classical nanoindentation and RPI were used to assess the deformation resistance of the control and PDB cases. Nanoindentation reveals a 14% lower Young's modulus ($p = 0.002$) and a 19% lower hardness ($p = 0.003$) in PDB samples (Fig. 5*A*, *B*). RPI was also used to investigate the bone's mechanical resistance.[51,52] RPI is a microindentation technique that cyclically loads the bone with an indenter in relation to a reference point. The RPI parameters showed significantly higher indentation depths in the PDB samples (Fig. 5*C*–*E*) with no change in the average energy dissipated (Fig. 5*F*). A previous study using RPI in this orientation found that bone with a lower modulus also had higher indentation depth values.[52] Thus, the indentation techniques reveal that the PDB cases have a lower modulus and less resistance to plastic deformation.

Fracture mechanics tests were performed on the hydrated cortices of control and PDB samples. The fracture toughness in terms of the linear-elastic stress intensity, *K*, was measured as a function of crack extension, Δa, to determine the crack growth resistance curve (ie, R-curve) (see Fig. 6*A*). The toughness of healthy bone is highly dependent on orientation, mainly due to different extrinsic mechanisms that are active in either orientation.

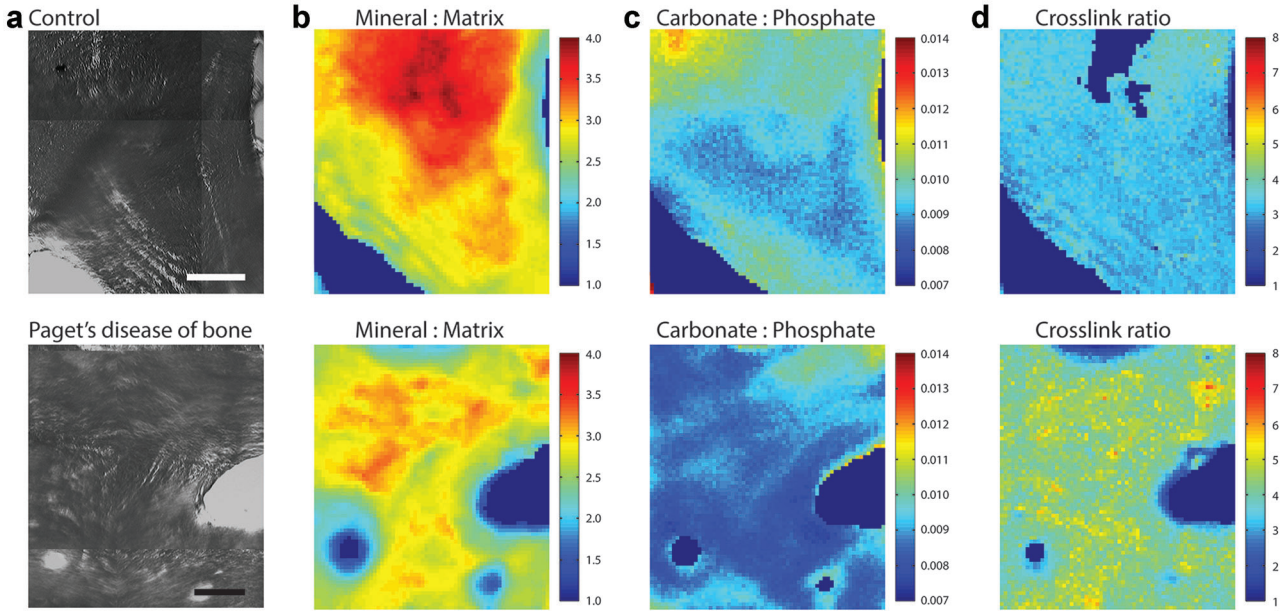

Fig. 3. Small length-scales: FTIR. The quality of the collagen and mineral components was assessed via FTIR mapping. (*A*) Spectra were collected at 6.25-μm intervals across a defined region of interest. (*B*) From the data, the mineral-to-matrix ratio was significantly 12% lower in the PDB cases ($p = 0.009$). (*C*) The carbonate-to-phosphate ratio was 15% lower in the PDB cases ($p = 0.003$) and (*D*) the collagen crosslink ratio was 15% higher in the PDB cases ($p = 0.040$). Scale bars = 100 μm. FTIR = Fourier transform infrared spectroscopy; PDB = Paget's disease of bone.

Therefore, fracture toughness is generally higher in the transverse orientation where crack deflection along the microstructural features is most active, in comparison to the longitudinal orientation, where this deflection mechanism is not favored because the osteons are parallel to the crack.[53,54] Because bone with PDB loses its parallel aligned Haversian systems, the bone could be expected to have a fracture toughness similar to the longitudinal orientation. However, our results indicate that the fracture toughness of the transversely-oriented control and PDB samples was not significantly different as measured through the intercept of the R-curve ($p = 0.34$), the slope of the R-curve in Fig. 6*A* ($p = 0.76$), and through the energy dissipated during RPI (Fig. 5*F*, $p = 0.06$).

To further investigate the fracture toughness measurements, we imaged the path of the crack via scanning electron microscopy during testing and synchrotron X-ray μCT after testing (Fig. 6*B*–*E*). Although there was no change in fracture toughness, we did observe the effect of the extreme changes in microstructural morphology on the crack path. Because of the normal microstructural orientation of the osteons, the crack takes a deflected path in control cases, which can account for the increase in bone toughness with crack extension (Fig. 6*B*, *D*).[53] However, the crack path in the PDB samples is straighter than the control cases and still contains crack bridges, which occur at interfaces within the microstructure such as the interface between bone packets and lamellae (Fig. 6*C*, *E*).

Discussion

Through the bowing, deformities, and fissure fractures observed in clinical cases, PDB has a clear effect on the bone's mechanical

Table 2. Static Histomorphometry

Histomorphometric indices	Control	PDB	Percent change (%)	*p*
Bone volume, BV/TV (%)	15.6 ± 5.8	41.5 ± 7.8	+266	<0.001
Trabecular thickness, Tb.Th (μm)	131.8 ± 36.2	129.0 ± 51.5	−2	n.s.
Trabecular number, Tb.N (mm^{-1})	1.21 ± 0.35	3.65 ± 1.35	+301	<0.001
Trabecular separation, Tb.Sp (μm)	792.9 ± 388.7	180.1 ± 65.4	−77	<0.001
Osteoid volume, OV/BV (%)	1.35 ± 1.62	10.54 ± 7.38	+807	<0.001
Osteoid surface, OS/BS (%)	16.3 ± 13.7	50.0 ± 18.4	+306	<0.001
Osteoblast number, N.Ob/B.Pm (mm^{-1})	0.62 ± 0.27	15.84 ± 8.71	+2548	<0.001
Osteoblast surface, Ob.S/BS (%)	0.96 ± 0.55	22.18 ± 12.46	+2302	<0.001
Osteoclast number, N.Oc/BS (mm^{-1})	0.03 ± 0.03	1.89 ± 0.81	+6000	<0.001
Osteoclast surface, Oc.S/BS (%)	0.31 ± 0.22	7.99 ± 3.76	+2548	<0.001

The static histomorphometry of the control and PDB cases was evaluated according to standards set by the ASBMR.[34] The values are reported as mean ± SD.

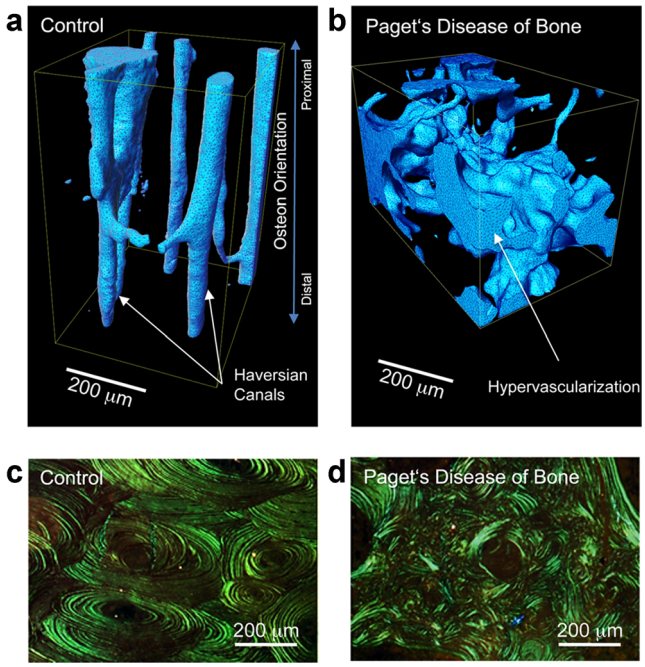

Fig. 4. Large length-scales: cortical microstructure. Synchrotron μCT and polarized light microscopy were used to observe changes at the osteonal length-scale in the cortical bone. (*A*) The 3D tomography reconstructions show that in control cases, the osteons have a predominant orientation with parallel-aligned Haversian canals, which is absent in (*B*) the PDB cases. Additionally, polarized light microscopy indicates that (*C*) the osteons in control cases have alternating light and dark lamellae reflecting normal collagen fiber orientation, whereas the (*D*) PDB cases are a mosaic of immature woven and lamellar bone. μCT = micro–computed tomography; PDB = Paget's disease of bone.

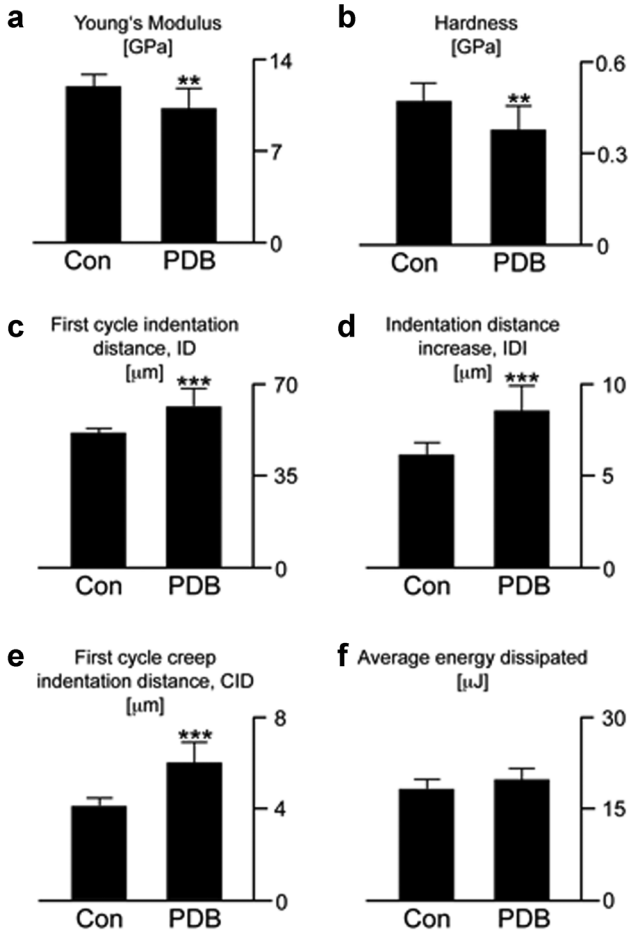

Fig. 5. Mechanical properties: Nanoindentation and RPI. Nanoindentation of the control and PDB cases reveals (*A*) a 14% lower modulus ($p = 0.002$) and (*B*) a 19% lower hardness in PDB ($p = 0.003$). RPI characterizes the bone's mechanical resistance by cyclically loading the bone with a microindenter in relation to a reference point. (*C–E*) The RPI parameters indicate significantly higher indentation depths in PDB (all $p < 0.001$), which supports the nanoindentation trends of a lower modulus and hardness. However, (*F*) the average energy dissipated was not significantly different ($p = 0.06$). Values reported as mean ± SD. RPI = reference point indentation; PDB = Paget's disease of bone.

integrity, which results from a combination of intrinsic mechanisms at small-length scales that generate/restrict plasticity and of extrinsic mechanisms at larger-length scales that interfere with the crack growth. Here, through a multiscale investigation of bone quality and mechanical properties in control and PDB cases, we investigate how the extreme changes to the multiscale bone structure (Fig. 1) lead to the pathological changes observed in the clinic.

In PDB cases, the bone quality was significantly altered at small-length scales. Specifically, the mineral content and distribution measured through qBEI (Fig. 2) and FTIR (Fig. 3) show that the PDB cases have a significantly lower degree of mineralization. This composition change directly relates to the significantly lower stiffness of the PDB tissue measured via nanoindentation and possibly also the higher indentation distance values measured via RPI[52] (Fig. 5), because in most biological materials, the Young's modulus (ie, stiffness) scales with mineral content.[55]

In addition to affecting the bone stiffness, the deviations in bone quality at small-length scales (Figs. 2, 3) influence how the diseased bone generates plastic deformation.[56,57] Indeed, the lower hardness and the deeper indentation values (Fig. 5) indicate that the pathological bone tissue will generate more plasticity than the control cases and suggests that the modifications to the quality of the tissue alter the intrinsic mechanisms within the structure (ie, fibrillar sliding and sacrificial bonding). Thus, the structural and compositional changes at small-length scales in PDB affect both the elastic (ie, stretching of bonds generating stiffness) and plastic (ie, permanent deformation promoting ductility and energy absorption) mechanical properties resulting in a lower stiffness and more plasticity.

In PDB cases, the bone quality was also significantly altered at larger-length scales. In the trabecular region of the iliac crest, the elevated bone turnover results in more trabeculae as reflected by the higher BV/TV and trabecular number[3] (Table 2). In the cortical compartment, the parallel aligned Haversian canals characteristic of healthy human bone are replaced by a patchwork of lamellar and woven bone in PDB cases, with less organized collagen fiber orientation[15–17] (Fig. 4). Thus, on the microstructural level, the sandwich structure of the iliac crest consisting of a trabecular core surrounded by dense cortical frame in control cases is replaced by

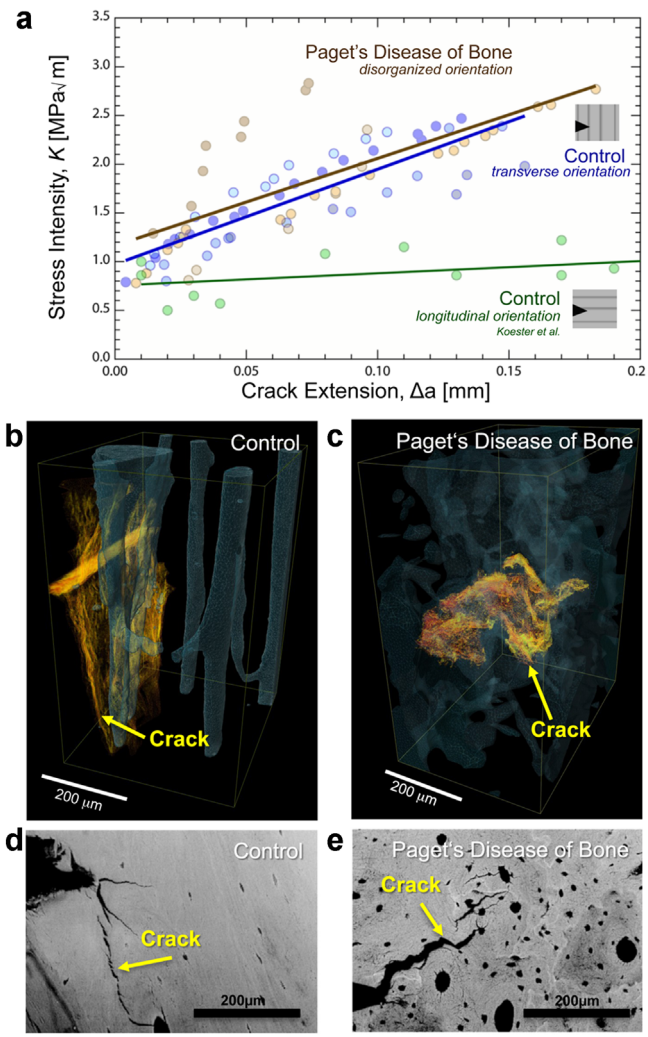

Fig. 6. Mechanical properties: fracture toughness and crack path. (*A*) The fracture toughness in terms of the linear-elastic stress intensity, *K*, of control and PDB cases was measured as a function of crack extension, Δa, which is called a crack growth resistance curve or *R*-curve. The fracture toughness of control (ie, transversely oriented) and PDB cases was not significantly different, as measured through the intercept ($p = 0.34$) and slope of the R-curve ($p = 0.76$). Because the PDB cases do not have a defined orientation for crack deflection due to their mosaic structure, the fact that the toughness is comparable to the transverse orientation and higher than the longitudinal orientation (which is also not optimized for crack deflection) is surprising.[53] Based on our observations (*B*, *C*) of the crack path after testing (via synchrotron X-ray computed microtomography) and (*D*, *E*) during testing (via scanning electron microscopy), (*B*, *D*) the control cases toughen extrinsically by deflecting along the interfaces of the osteons, whereas (*C*, *E*) the PDB cases take a straighter crack path through the disordered structure with large crack bridges. PDB = Paget's disease of bone.

a dense clumsy bone structure that lacks a well-defined directional orientation of collagen fibers and osteons.

Even though PDB resulted in significant changes to the structure at large-length scales, the fracture toughness of the diseased bone measured through the energy dissipated during RPI (Fig. 5) and the crack-growth toughness (Fig. 6) during fracture mechanics experiments was not significantly different in comparison to the transversely-oriented controls. This is in line with some of the limitations of this study, which are (1) the limited number of fracture toughness samples, which restricts the statistical comparisons, and (2) that the embedding and infiltration procedures may limit the effects of sample rehydration, which affects the mechanical property measurements. Although future studies with larger sample sets are required to precisely distinguish a difference in fracture toughness between the control and PDB samples, there was still a clearly higher fracture toughness in the transversely-oriented controls and the PDB samples in comparison to the longitudinally-oriented bone, which has a comparatively weak resistance to crack growth.[53]

Therefore, in both the transversely-oriented controls and the PDB samples, there appears to be a form of extrinsic resistance to crack growth. In the controls, the mechanical resistance to crack propagation is primarily derived through crack deflection (see Fig. 6), which has been shown to increase fracture toughness.[53] In PDB, the crack deflection mechanism is lost, resulting in straighter crack paths (see Fig. 6) due to the microstructural alterations. However, one possible route to generate further mechanical resistance would be through increased plastic deformation. Thus, the fracture toughness measurements may indicate that the bone's intrinsic resistance (ie, lower mineralization leading to lower hardness, more plasticity) compensates for the loss in the extrinsic crack deflection mechanism (ie, due to the loss in the parallel-aligned Haversian systems). This increase in plasticity would act to absorb energy during crack propagation, leading to an increased fracture toughness and is supported by studies on other low-mineralized tissues that have also found significant plastic deformation.[22,56] Thus, even though PDB samples lose their microstructural orientation, which is critical to the fracture toughness of healthy bone, the altered, heterogeneous structure characteristic of the pathological tissue may compensate by generating more intrinsic plasticity to resist crack growth.

In terms of clinical relevance, bone disorders associated with an underlying imbalance in the remodeling process can lead to increased fracture risk, particularly when the disorder creates structural and compositional changes. Clearly, the modifications to the bone tissue caused by the high bone turnover in PDB uniquely affect the bone structure, leading to a higher bone volume, lower, heterogeneous mineral content/distribution, significantly younger tissue age, and loss in lamellar osteonal bone structure. These characteristics of the bone structure and composition of PDB are not associated with known bone fragility in other diseases. However, even though the characteristics of the Paget bone structure are contrary to other bone disorders *with* fracture risk, it is necessary to recognize the impact of PDB on the mechanical integrity.

The specific effects on the pathological bone tissue, in particular bone deformities and fissure fractures, can now be further clarified from the present multiscale characterization of the bone structure and mechanical properties. Indeed, the excess amount of osteoid and mineralized bone produced in PDB leads to deformities and bowing in clinical PDB cases, where incomplete or "fissure fractures" occur in deformed load-bearing tissue.[28,30] Here, our experimental data, revealing a lower spatially-resolved mineral content and tissue age of the bone with a corresponding lower stiffness and lower resistance to deformation, could directly account for the occurrence of harmful bone deformities in patients suffering from PDB. The deformities can in turn lead to osteoarthritis due to the gait problems encountered when deformities occur in load-bearing limbs.[58]

The other interesting phenomenon is the presence of subcritical (ie, stable) cracks, so-called fissure fractures, in PDB. The fissure fractures most likely occur because of the bone deformities/bowing, but the fact that these fractures remain in the tissue and do not completely cause bone failure is in line with the same propensity for the altered structure to resist crack growth through plastic deformation. In this way, the altered composition (ie, the reduced mineral content) has a negative impact on the bone stiffness (ie, causes bowing/deformity), but compensates for the reorganized bone microstructure by generating plastic deformation to resist the growth of cracks allowing stable fissure cracks. In this connection, although bone fracture is an important issue in patients with PDB and stable cracks do occur, our fracture toughness data suggests that the material properties of the bone may compensate to a certain degree to prevent complete bone fracture.

In conclusion, on a set of human bone biopsies from control and PDB cases, we found that the high bone turnover associated with PDB causes a significantly lower mineral content and tissue age. At larger structural-length scales, the trabecular region is known to become densified, whereas the cortex loses the lamellar Haversian osteon structure with its regular arrangement, which is replaced by a mosaic of immature woven and lamellar bone. Through the indentation measurements presented here, the structural changes at small-length scales clearly reduce the stiffness and promote plastic deformation in PDB cases. In turn, the loss of the osteonal structures should deteriorate the fracture toughness, but the larger degree of plastic deformation at small-length scales compensates for the lack of structure and may be the reason for the maintained fracture toughness presented here. Therefore, the alterations to the structure in PDB produce bowing/deformities, namely from the low mineral content, but may also improve the mechanical integrity of the tissue by promoting plastic deformation to stop the growth of cracks, leading to the presence of stable fissure fractures characteristic of the disease.

Disclosures

All authors state that they have no conflicts of interest.

Acknowledgements

This study was supported by the German Research Foundation (DFG) under grants BU 2562/2-1 and BU 2562/1-1. We acknowledge use of the μCT beam line 8.3.2 at the Advanced Light Source (ALS) synchrotron at Lawrence Berkeley National Laboratory (LBNL), Berkeley, CA, USA. The Advanced Light Source is supported by the Director, Office of Science, Office of Basic Energy Sciences, of the U.S. Department of Energy under Contract No. DE-AC02-05CH11231. We thank Dr. Björn Jobke (DKFZ, Heidelberg) for plain film images of PDB.

Authors' roles: EAZ, ROR, and BB designed the study. EAZ, TK, HAB, BP, BG, and BB performed the experiments. EAZ, TK, HAB, BP, BG, MA, ROR, and BB analyzed the data. EAZ, HAB, JZ, MH, MA, ROR, and BB contributed reagents or analytic tools. MH and JZ gave technical support and conceptual advice. EAZ and BB wrote the manuscript. EAZ, TK, HAB, BP, BG, JZ, MH, MA, ROR, and BB approved the final version of the manuscript.

References

1. Paget J. On a form of chronic inflammation of bones (Osteitis Deformans). Med Chir Trans. 1877;60:37–64. 9.
2. Davie M, Davies M, Francis R, Fraser W, Hosking D, Tansley R. Paget's disease of bone: a review of 889 patients. Bone. 1999;24(5):11S–2S.
3. Seitz S, Priemel M, Zustin J, et al. Paget's disease of bone: histologic analysis of 754 patients. J Bone Miner Res. 2009;24(1):62–9.
4. Corral-Gudino L, Borao-Cengotita-Bengoa M, Del Pino-Montes J, Ralston S. Epidemiology of Paget's disease of bone: a systematic review and meta-analysis of secular changes. Bone. 2013;55(2):347–52.
5. Gennari L, Merlotti D, Martini G, Nuti R. Paget's disease of bone in Italy. J Bone Miner Res. 2006;21(S2):P14–21.
6. Pestka JM, Seitz S, Zustin J, Püschel K, Amling M, Barvencik F. Paget disease of the spine: an evaluation of 101 patients with a histomorphometric analysis of 29 cases. Eur Spine J. 2012;21(5):999–1006.
7. Guyer PB. Paget's disease of bone: the anatomical distribution. Metab Bone Dis Relat Res. 1981;3(4–5):239–41.
8. Siris ES, Feldman F. Clinical vignette: natural history of untreated Paget's disease of the tibia. J Bone Miner Res. 1997;12(4):691–2.
9. Ralston SH. Paget's disease of bone. N Engl J Med. 2013;368(7):644–50.
10. Lyles KW, Siris ES, Singer FR, Meunier PJ. A clinical approach to diagnosis and management of Paget's disease of bone. J Bone Miner Res. 2001;16(8):1379–87.
11. Delmas PD, Meunier PJ. The management of Paget's disease of bone. N Engl J Med. 1997;336(8):558–66.
12. Mirra JM, Brien EW, Tehranzadeh J. Paget's disease of bone: review with emphasis on radiologic features, part I. Skeletal Radiol. 1995;24(3):163–71.
13. Shankar S, Hosking DJ. Biochemical assessment of Paget's disease of bone. J Bone Miner Res. 2006;21(S2):P22–7.
14. Jobke B, Milovanovic P, Amling M, Busse B. Bisphosphonate-osteoclasts: changes in osteoclast morphology and function induced by antiresorptive nitrogen-containing bisphosphonate treatment in osteoporosis patients. Bone. 2014;59:37–43.
15. Meunier PJ, Coindre JM, Edouard CM, Arlot ME. Bone histomorphometry in Paget's disease. Quantitative and dynamic analysis of pagetic and nonpagetic bone tissue. Arthritis Rheum. 1980;23(10):1095–103.
16. Rebel A, Basle M, Pouplard A, Malkani K, Filmon R, Lepatezour A. Bone tissue in Paget's disease of bone ultrastructure and immunocytology. Arthritis Rheum. 1980;23(10):1104–14.
17. Giannini C, Siliqi D, Bunk O, et al. Correlative light and scanning X-ray scattering microscopy of healthy and pathologic human bone sections. Sci Rep. 2012;2:435.
18. Zimmermann EA, Schaible E, Bale H, et al. Age-related changes in the plasticity,toughness of human cortical bone at multiple length scales. Proc Natl Acad Sci U S.A. 2011;108(35):14416–21.
19. Busse B, Bale HA, Zimmermann EA, et al. Vitamin D deficiency induces early signs of aging in human bone, increasing the risk of fracture. Sci Transl Med. 2013;5(193):193ra88.
20. Barth HD, Zimmermann EA, Schaible E, Tang SY, Alliston T, Ritchie RO. Characterization of the effects of x-ray irradiation on the hierarchical structure and mechanical properties of human cortical bone. Biomaterials. 2011;32(34):8892–04.
21. Carriero A, Zimmermann EA, Paluszny A, et al. How tough is brittle bone? Investigating osteogenesis imperfecta in mouse bone. J Bone Miner Res. 2014;29(6):1392–401.
22. Launey ME, Buehler MJ, Ritchie RO. On the mechanistic origins of toughness in bone. Annu Rev Mater Res. 2010;40(1):25–53.
23. Melton LJ, Tiegs RD, Atkinson EJ, O'Fallon WM. Fracture risk among patients with Paget's disease: a population-based cohort study. J Bone Miner Res. 2000;15(11):2123–8.
24. Van Staa TP, Selby P, Leufkens HGM, Lyles K, Sprafka JM, Cooper C. Incidence and natural history of Paget's disease of bone in England and Wales. J Bone Miner Res. 2002;17(3):465–71.
25. Gold DT, Boisture J, Shipp KM, Pieper CF, Lyles KW. Paget's disease of bone and quality of life. J Bone Miner Res. 1996;11(12):1897–04.
26. Langston AL, Campbell MK, Fraser WD, MacLennan GS, Selby PL, Ralston SH. Randomized trial of intensive bisphosphonate treatment versus symptomatic management in Paget's disease of bone. J Bone Miner Res. 2010 Jan 1;25(1):20–31.

27. Dove J. Complete fractures of the femur in Paget's disease of bone. J Bone Joint Surg Br. 1980 Feb;62-B(1):12–7.
28. Cushing FR, Bone HG. Radiographic diagnosis and laboratory evaluation of Paget's disease of bone. Clin Rev Bone Miner Metab. 2002;1(2):115–34.
29. Grundy M. Fractures of the femur in Paget's disease of bone their etiology and treatment. J Bone Joint Surg Br. 1970;52(2):252–63.
30. Redden JF, Dixon J, Vennart W, Hosking DJ. Management of fissure fractures in Paget's disease. Int Orthop. 1981;5(2):103–6.
31. Seitz S, Priemel M, von Domarus C, et al. The second most common bone disease: a review on Paget's disease of bone. Eur J Trauma Emerg Surg. 2008;34(6):549–53.
32. Priemel M, von Domarus C, Klatte TO, et al. Bone mineralization defects and vitamin D deficiency: histomorphometric analysis of iliac crest bone biopsies and circulating 25-hydroxyvitamin D in 675 patients. J Bone Miner Res. 2010 Feb 1;25(2):305–12.
33. Koehne T, Vettorazzi E, Küsters N, et al. Trends in trabecular architecture and bone mineral density distribution in 152 individuals aged30-90 years. Bone. 2014 Sep;66:31–8.
34. Dempster DW, Compston JE, Drezner MK, et al. Standardized nomenclature, symbols, and units for bone histomorphometry: a 2012 update of the report of the ASBMR Histomorphometry Nomenclature Committee. J Bone Miner Res. 2013;28(1):2–17.
35. Boyde A, Maconnachie E, Reid SA, Delling G, Mundy GR. Scanning electron microscopy in bone pathology: review of methods, potential and applications. Scan Electron Microsc. 1986; (Pt 4):1537–54.
36. Boyde A, Travers R, Glorieux FH, Jones SJ. The mineralization density of iliac crest bone from children with osteogenesis imperfecta. Calcif Tissue Int. 1999;64(3):185–90.
37. Skedros JG, Bloebaum RD, Bachus KN, Boyce TM, Constantz B. Influence of mineral content and composition on graylevels in backscattered electron images of bone. J Biomed Mater Res. 1993;27(1):57–64.
38. Roschger P, Plenk H Jr, Klaushofer K, Eschberger J. A new scanning electron microscopy approach to the quantification of bone mineral distribution: backscattered electron image grey-levels correlated to calcium K alpha-line intensities. Scanning Microsc. 1995;9(1):75–86.
39. Koehne T, Marshall RP, Jeschke A, Kahl-Nieke B, Schinke T, Amling M. Osteopetrosis, osteopetrorickets and hypophosphatemic rickets differentially affect dentin and enamel mineralization. Bone. 2013 Mar;53(1):25–33.
40. Roschger P, Paschalis EP, Fratzl P, Klaushofer K. Bone mineralization density distribution in health and disease. Bone. 2008 Mar;42(3):456–66.
41. Boskey A, Pleshko Camacho N. FT-IR imaging of native and tissue-engineered bone and cartilage. Biomaterials. 2007;28(15):2465–78.
42. Paschalis EP, Verdelis K, Doty SB, Boskey AL, Mendelsohn R, Yamauchi M. Spectroscopic characterization of collagen cross-links in bone. J Bone Miner Res. 2001;16(10):1821–8.
43. Farlay D, Panczer G, Rey C, Delmas PD, Boivin G. Mineral maturity and crystallinity index are distinct characteristics of bone mineral. J Bone Miner Metab. 2010;28(4):433–45.
44. Regelsberger J, Milovanovic P, Schmidt T, et al. Changes to the cell, tissue and architecture levels in cranial suture synostosis reveal a problem of timing in bone development. Eur Cell Mater. 2012 Dec;24;441–58.
45. ASTM E1820-09. Standard Test Method for Measurement of Fracture Toughness [Internet]. West Conshohocken, PA: ASTM International; 2009; [cited 2014 Oct 22]. Available from:http://www.astm.org/DATABASE.CART/HISTORICAL/E1820-09.htm.
46. Cotterell B, Rice J. Slightly curved or kinked cracks. Int J Fract. 1980;16(2):155–69.
47. Farlay D, Duclos M-E, Gineyts E, et al. The ratio 1660/1690 cm^{-1} measured by infrared microspectroscopy is not specific of enzymatic collagen cross-links in bone tissue. PloS One. 2011;6(12):e28736.
48. Garnero P, Gineyts E, Schaffer AV, Seaman J, Delmas PD. Measurement of urinary excretion of nonisomerized and β-isomerized forms of type I collagen breakdown products to monitor the effects of the bisphosphonate zoledronate in Paget's disease. Arthritis Rheum. 1998;41(2):354–60.
49. Ascenzi M-G, Ascenzi A, Benvenuti A, Burghammer M, Panzavolta S, Bigi A. Structural differences between "dark" and "bright" isolated human osteonic lamellae. J Struct Biol. 2003;141(1):22–33.
50. Boyde A, Bianco P, Portigliatti Barbos M, Ascenzi A. Collagen orientation in compact bone: I. A new method for the determination of the proportion of collagen parallel to the plane of compact bone sections. Metab Bone Dis Relat Res. 1984;5(6):299–307.
51. Diez-Perez A, Güerri R, Nogues X, et al. Microindentation for in vivo measurement of bone tissue mechanical properties in humans. J Bone Miner Res. 2010 Aug;25(8):1877–85.
52. Thurner PJ, Erickson B, Turner P, et al. The effect of NaF in vitro on the mechanical and material properties of trabecular and cortical bone. Adv Mater. 2009 Jan 26;21(4):451–7.
53. [was 46] Koester KJ, Ager JW, Ritchie RO, The true toughness of human cortical bone measured with realistically short cracks. Nat Mater. 2008;7(8):672–7.
54. Zimmermann EA, Barth HD, Ritchie RO. The multiscale origins of fracture resistance in human bone and its biological degradation. JOM 1989. 2012 Apr;64(4):486–93.
55. Currey JD. The mechanical consequences of variation in the mineral content of bone. J Biomech. 1969;2(1):1–11.
56. Jager I, Fratzl P. Mineralized collagen fibrils: a mechanical model with a staggered arrangement of mineral particles. Biophys J. 2000;79(4):1737–46.
57. Donnelly E, Boskey AL, Baker SP, van der Meulen MCH. Effects of tissue age on bone tissue material composition and nanomechanical properties in the rat cortex. J Biomed Mater Res A. 2010;92(3):1048–56.
58. Siris ES. Paget's disease of bone. J Bone Miner Res. 1998 Jul 1;13(7):1061–5.